Proton MR Spectroscopy of the Normal Human Prostate with an Endorectal Coil and a Double Spin-Echo Pulse Sequence

Arend Heerschap, Gerrit J. Jager, Marinette van der Graaf, Jelle O. Barentsz, Sjef H. J. Ruijs

This report describes the use of an endorectal coil and a double spin-echo pulse sequence for localized ^{1}H MR spectroscopy of the normal prostate in volunteers. The spectra showed well-resolved signals for citrate, (phospho)choline, and creatine protons. Additional signals were assigned to taurine and myoinositol protons. *J* modulation of the main and outer peaks of citrate could be monitored *in vivo*. Apparent relaxation times T_1 and T_2 have been estimated for the methyl protons of cholines and creatine. An effective T_1 relaxation time was estimated for the main peaks of the citrate multiplet. Ratios of the integrals of these resonances have been evaluated, and tissue contents of choline and creatine were estimated using the H_2O signal as an internal reference. Spectroscopic imaging experiments revealed a lower relative citrate signal in central parts of the prostate than in peripheral parts.

Key words: human prostate; magnetic resonance spectroscopy; metabolites; spectroscopic imaging.

INTRODUCTION

Proton magnetic resonance spectroscopy (^{1}H MRS) has been mostly applied to the brain in human studies. To extend its use to other parts of the human body seems less trivial. Problems involved in abdominal application of ^{1}H MRS are related to the deep location and movement of some tissues of interest. Furthermore, dominating triglyceride signals, either from the target tissue itself or from adjacent adipose tissue, often obscure resonances of relevant metabolites.

With the advent of endorectal RF coils (1, 2), the potential of ^{1}H MR of the human prostate has improved substantially, and several groups have explored the use of such coils to obtain ^{1}H MR spectra of the human prostate (3–5). The most prominent metabolite signal in these spectra is that of citrate, a compound abundantly present in the healthy prostate. The tissue content of citrate has been reported as a potential marker for prostate pathology, in particular to discriminate between the presence of adenocarcinomas and benign prostate hyperplasia (BPH) (6–13). The intensity of the methyl proton signal of (phospho)cholines in ^{1}H MR spectra of the prostate may also serve this purpose (5, 12, 13). Localized ^{1}H MRS of the human prostate based on magnet field gradient techniques has been initiated with use of the stimulated-echo acquisition mode (STEAM) sequence (4, 9, 13) and the point-resolved spectroscopy (PRESS) sequence (5, 14).

In this study, we report on the application of a double spin-echo (or PRESS) sequence (15, 16) in combination with endorectal coils in ^{1}H MRS of the prostate of healthy volunteers. At a *TE* of 135 ms, well-resolved spectra were obtained showing major signals for citrate, choline compounds, and creatine. Minimal contamination of these spectra with broad components facilitated the quantitation of metabolite levels. Furthermore, high-quality ^{1}H MR spectra were obtained in multiple locations of the human prostate by extending PRESS volume localization with phase-encoding gradients to collect a spectroscopic imaging (SI) data set.

MATERIALS AND METHODS

Volunteers

This study was approved by the local ethical committee. After informed consent was given 12 volunteers participated in this study. Of these volunteers, eight were examined with single volume localization, of which three were investigated twice. Four were examined in studies using SI. The ages of the volunteers ranged from 25 to 46 years. None of the volunteers had a history of genitourinary disease or showed any signs of clinical prostate disease. MR images obtained of the prostates were interpreted as being normal. The volunteers were examined in the supine position. A belt was applied around the lower abdomen with slight compression to reduce respiratory motion. No antiperistaltic drugs were used.

MR Imaging

MR examinations were performed on a 1.5 T MR system (Magnetom SP, Siemens, Erlangen, Germany) using a body RF coil for excitation. For MR signal reception, a disposable endorectal probe (MEDRAD®, Pittsburgh, PA) holding a surface coil with approximate length of 75 mm and width of 35 mm was inserted. The probe was inflated with 50 to 100 ml of air to ensure tight positioning of the coil adjacent to the prostate. To visualize the prostate, multiple-slice MR imaging was performed in three orthogonal planes using a turbo spin-echo sequence (slice thickness, 5 mm; 1-mm interslice distance; field of view, 260 mm; matrix, 260 × 512; acquisitions, 2; *TE*, 160 ms; *TR*, 2940 ms).

MRM 37:204–213 (1997)

From the Department of Radiology, University Hospital Nijmegen, Nijmegen, The Netherlands.

Address correspondence to: Arend Heerschap, Ph.D., Department of Radiology, Medical Faculty, University Hospital Nijmegen, P.O. Box 9101, 6500 HB Nijmegen, The Netherlands; email: a.heerschap@rdiag.azn.nl.

Received April 1, 1996; revised July 23, 1996; accepted August 8, 1996.

This work was supported by the Dutch Cancer Society.

0740-3194/97 $3.00

Single-Voxel MRS

On the basis of these images, volumes were selected for localized ^{1}H MRS using a double spin-echo slice-selective sequence (90° - τ - 180° - T - 180° - (T − τ) - Acquisition)with *TE*s (2 T) between 30 and 270 ms. The delay time τ was 11 ms. The length of the sinc-shaped RF pulses was 2.56 ms, and the bandwidth of the 180° pulses was adjusted to select the same effective slice thickness as for the 90° pulse. The slice-selective gradients were 2.67 mT/m, and EXORCYCLE phase cycling was applied. Field homogeneity was optimized for the selected volume using the resonance of water protons. For the detection of metabolite signals, a chemical-shift–selective method (17) was used to suppress the water resonance and 2 K data points were acquired with a spectral width of 1000 Hz. The nominal dimensions of the voxels were 1.5 × 1.5 × 1.5 cm (3.4 cc), except in two cases in which voxels with nominal dimensions of 1.6 × 1.6 × 1.6 cm (4.1 cc) and 1.8 × 1.8 × 1.8 cm (5.8 cc) were selected. The scan *TR* ranged from 1.6 to 4.5 s, and the number of scans from 96 to 256. In addition, a spectrum without water suppression was obtained for eddy-current correction and for referencing purposes.

To estimate apparent T_2 relaxation times of metabolite proton spins *in vivo*, spectra were recorded at four different *TE*s between 65 and 270 ms. For the estimation of the apparent T_2 relaxation time of water proton spins, seven spectra were recorded without water-resonance suppression at *TE*s between 30 and 270 ms.

Inversion-recovery experiments to obtain apparent T_1 relaxation times were performed by the same pulse sequence used for localization, preceded by a nonselective 180° inversion pulse (650 μs). The *TE* was 135 ms and the *TR* 3 s. Five or six spectra were recorded at different delay times between the inversion pulse and the localization sequence ranging from 50 to 1000 ms. In the same way, inversion-recovery experiments were performed without water suppression. The *TR* was set to 6 s, and delay times ranged from 50 to 2500 ms (number of delay times investigated was six to eight).

Besides these experiments with volunteers, inversion-recovery experiments were also performed on a phantom (described below). Thirteen measurements were performed with inversion-delay times between 40 and 1600 ms at a *TR* of 6 s.

Spectroscopic Imaging (SI)

In the SI experiments, a transversal slice of 10- or 11-mm thickness, 40 mm in the left-right and 30 mm in the anterior-posterior direction, was selected for localized ^{1}H MRS by the double spin-echo sequence described above with a *TE* of 135 ms. In these experiments, τ was 14.5 ms, the pulse lengths were 5.12 ms, and the slice-selection gradient in the *z* direction was 3 mT/m and in the other directions 1.4 mT/m. Gradients for phase encoding in two directions were applied during 1 ms in the τ period, to obtain a set of SI data within the preselected volume. The field of view was 160 mm. Data were encoded in a 16 × 16 matrix, resulting in nominal voxels of about 1.0 cc. For the spectral dimension, 1 K data points were acquired with a spectral width of 1 kHz. A total of 512 scans (two scans per phase-encoding step) were acquired with a *TR* of 1.6 s, resulting in an acquisition time of 13.6 min. For eddy-current correction as well as referencing purpose, an SI experiment without water suppression was performed.

Phantom

To test the performance of MRS acquisition methods, a phantom was used. It consisted of a glass sphere with an outer diameter of 10 cm filled with a citrate solution prepared according to the average composition of expressed human prostatic fluid as reported by Kavanagh (18). It contained 90 m*M* sodium citrate, 8.8 m*M* $ZnCl_2$, 16.7 m*M* $MgCl_2$, 18.8 m*M* $CaCl_2$, and 63 m*M* KCl at pH 6.7. For referencing and phasing purposes, 13.6 m*M* glycine and 10 m*M* sodium acetate were added. The sphere was placed in a container filled with sunflower oil, to mimic the presence of periprostatic fat, which was positioned on the endorectal surface coil.

Postprocessing

Postprocessing of single volume measurements consisted of zero-filling to 4 K data points and filtering as indicated in the figures. Eddy-current correction was performed according to Klose (19) by a software procedure provided by the manufacturer. After this procedure, usually only minor phase correction was necessary.

In the case of SI, postprocessing consisted of Fourier transformation to spatial and frequency dimensions applying zero-filling to 2 K data points and a Gaussian filter for the frequency dimension. No *k*-space filtering was used. Eddy-current correction was performed as for the single-voxel measurements.

For fitting of signals in the frequency domain, NMR1 software (New Mothods Research, Inc., Syracuse, New York) was used. Apparent T_1 and T_2 relaxation-time values were derived by fitting the integrals of resonances to a single exponential function.

Average values are presented with standard deviations (±SD). Chemical shifts are given in parts per million (ppm).

RESULTS

Single-Volume Measurements

Spatial Origin of Spectra. By histology, the most simple subdivision of the prostate gland is in a central part (including transition-zone tissue) and a peripheral part, of which the latter part occupies about 70% of the normal prostate gland (20). To minimize signal contributions of periprostatic triglycerides, the volumes for MRS in this study were located in the central part of the prostate mainly containing central-zone/transition-zone tissue. From inspection of the MR images, the contribution of peripheral zone tissue to the selected volumes was estimated to be between 15 and 25% for nominal volumes of 3.4 cc. In two examinations, with nominal voxels of 4.1 and 5.8 cc the contribution of the peripheral zone to the selected volume was estimated to be 30 to 40%. Because a part of the peripheral zone included in the voxels was

closest to the endorectal surface coil, the actual contribution of signal intensity from this zone to the spectra is somewhat larger.

Homogeneity. In the present volunteer studies, we encountered few problems with prostate movement. If tissue movement occurs, this usually becomes manifest during the shimming procedure. One examination failed because of bad shimming results. Shimming values of all other 10 single-voxel examinations performed at a *TE* of 135 ms ranged from 3.5 to 10 Hz (full-width-half-maximum) with an average value of 6.2 ± 1.8 Hz.

Assignment of Spectral Components. Figure 1 shows a water-resonance image of a transversal slice through the prostate of a volunteer also displaying the outline of the voxel selected for MRS. The spectrum obtained from this voxel at a *TE* of 135 ms is shown in Fig. 2. Assignments are indicated in the spectrum. These are based on previous high-resolution NMR studies of perchloric acid extracts of prostate specimens (12). The most dominating metabolite resonance in the spectrum originates from citrate. At 1.5 T, the four proton spins of citrate behave as a strongly coupled AB system with nearly identical chemical shifts showing four resonances of which the two central ones are most intense at the present experimental conditions (14). *In vivo,* usually only one peak is visible containing both these central components. However, at shimming values of about 5 Hz (or less) the separate resonance components of citrate start to get resolved (see below). In addition to citrate resonances, all spectra showed peaks that could be assigned to the methyl protons of creatine and cholines. When referencing the creatine resonance to a chemical-shift position of 3.03 ppm, we find in spectra obtained at $TE = 135$ ms an average position ($n = 10$) for the choline peak at 3.21 ± 0.01 ppm, for the central position of citrate at 2.63 ± 0.01 ppm, and for the position of the water resonance at 4.68 ± 0.02 ppm. According to the extract studies, the choline peak originates mainly from phosphocholine and choline compounds. Resonances of taurine, inositol, ethanolamine, and polyamine protons may also contribute to signal intensity at 3.20 to 3.25 ppm (12, 13). The spectrum in Fig. 2 shows very little contribution of triglyceride signals between 1.7 and 0.5 ppm. In some of the spectra, signals in this region were more intense. These likely originate from periprostatic fat as verified by taking spectra of voxels located more to the periphery of the prostate, which showed an increased intensity of these resonances. In the spectra with minimal triglyceride signals, no indication for a signal of lactate was observed, which should be visible as an inverted doublet at about 1.33 ppm at a *TE* of 135 ms. At this *TE,* occasionally some additional weak resonances are observable that we tentatively assign, on the basis of prostate-extract studies (12), to protons of taurine (3.2 to 3.4 ppm), glutamate/glutamine (2.0 to 2.5 ppm) and inositol (3.54 ppm). These become better discernible at shorter *TE*s. See for instance the spectra in Fig. 3 obtained at *TE*s of 100 and 65 ms. At *TE*s between 65 and 100 ms, it is still possible to obtain spectra with resolved resonances for citrate, cholines and creatine, but for spectra at *TE* below 65 ms, resolution becomes worse, and therefore these spectra are more difficult to analyze. Usually, there is more signal contribution of triglycerides between 1.7 and 0.5 ppm at shorter *TE*s.

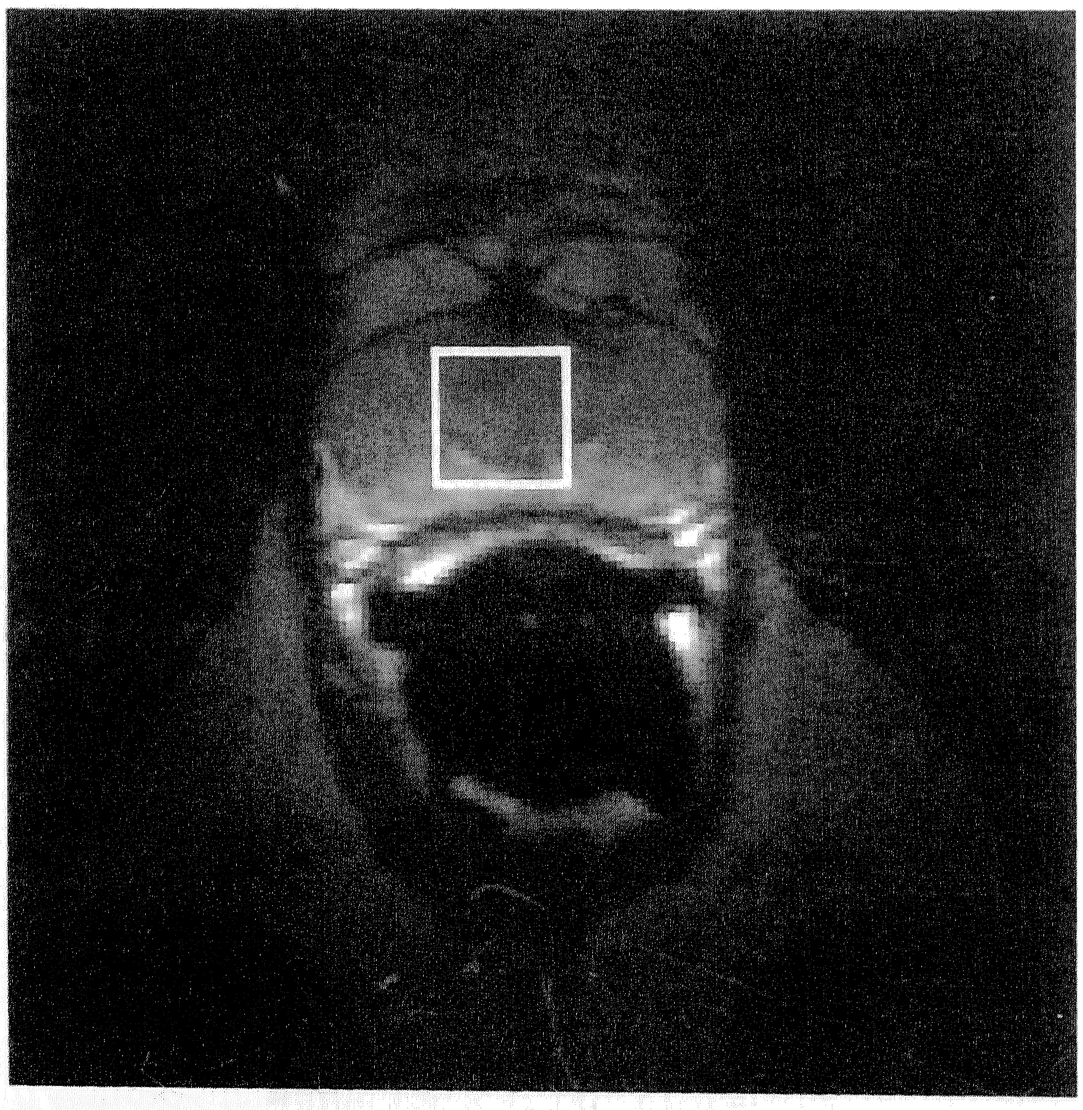

FIG. 1. Transversal MR image (T_2-weighted) showing the prostate of a 28-year-old volunteer. The volume selected for ^{1}H MRS is indicated by a box. It has a nominal volume of 3.4 cc (1.5 × 1.5 × 1.5 cm).

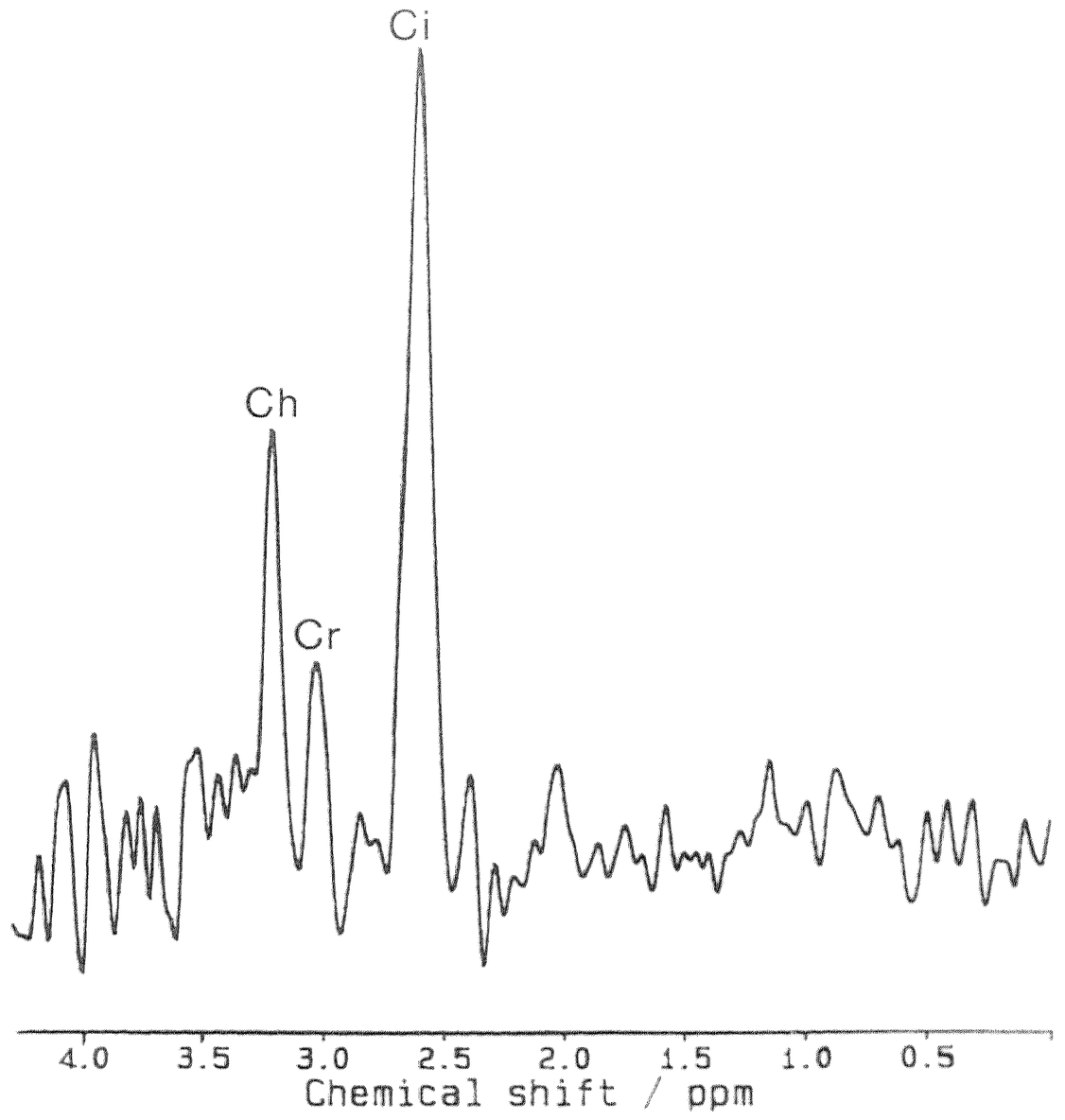

FIG. 2. ^{1}H MR spectrum of the volume shown in Fig. 1. This spectrum has been obtained with a *TE* of 135 ms, a *TR* of 1600 ms, and 256 scans. The half-width of the water resonance was 6 Hz. Zero-filling to 4 K and a Gaussian filter (maximum at 96 ms and half-width 148 ms) was applied to the free induction decay before Fourier transformation. No baseline correction was used. The indicated resonance assignments are Ci for the central citrate component, Cr for the methyl protons of creatine, and Ch for the methyl protons of (phospho)choline.

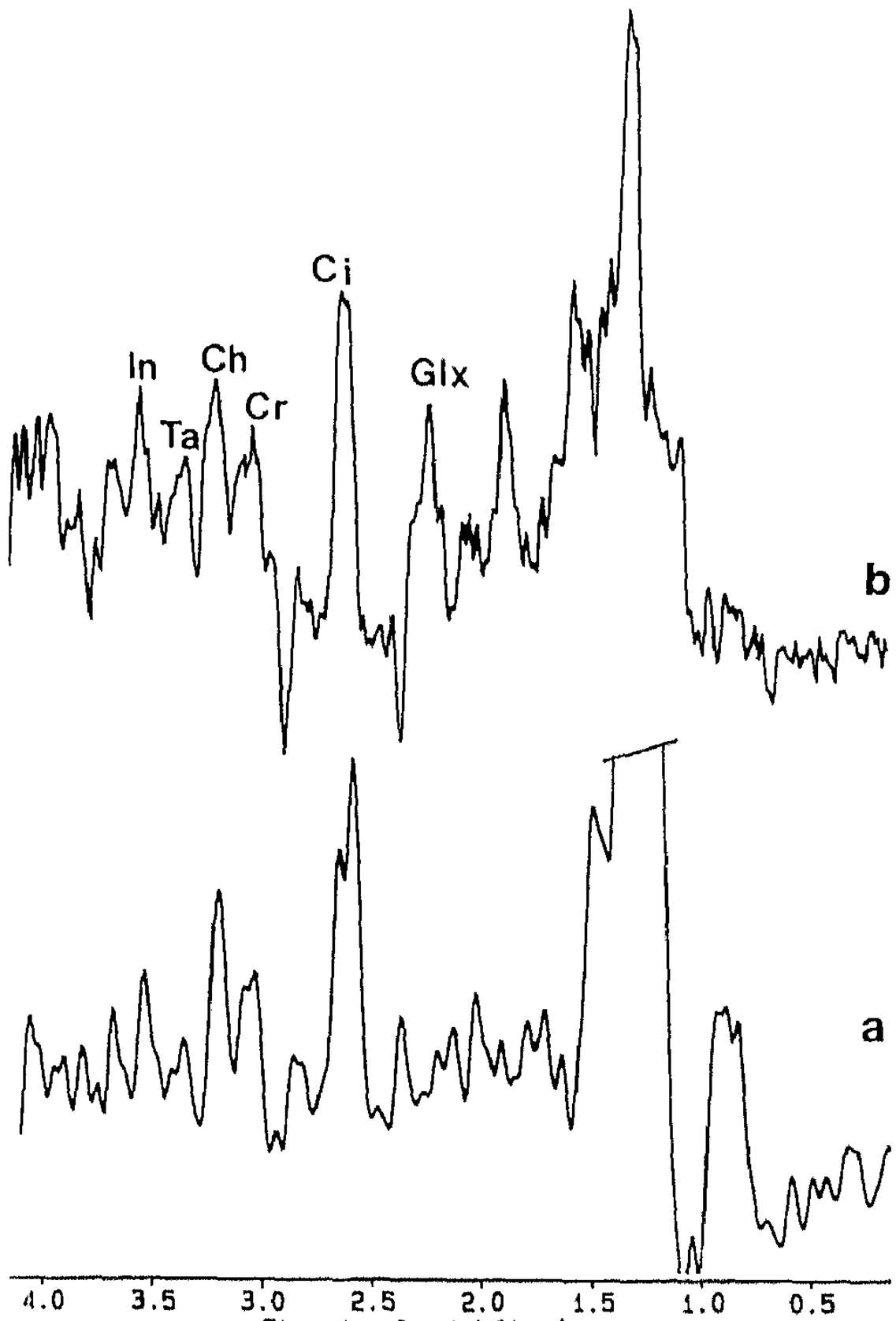

FIG. 3. MR spectra of the prostate of two volunteers obtained at different *TE*s. Nominal volumes were 3.4 cc. *TR* was 2000 ms. Processing was performed as for Fig. 2. Ta, taumine; In, inositol; Glx, glutamine/glutamate. Further details: (a) *TE* = 100 ms. Gaussian filter with maximum at 96 ms and half-width 160 ms. (b) *TE* = 65 ms. Gaussian filter with maximum at 160 ms and half-width 160 ms.

J Modulation of the Citrate Signal In Vivo. At shimming values of about 5 Hz width for the water resonance at half height, occasionally it became possible to observe the smaller outer signals of citrate at approximately 15 to 16 Hz from the central peaks. Figure 4 shows the spectral region between 2.2 and 3.3 ppm with the citrate resonances at various *TE*s. The outer peaks and the splitting of the main peak of citrate, at *TE*s of 135 ms and more, are well visible. As described previously (14), the main citrate component shows slow modulation at 1.5 T, both *in vitro* and *in vivo*. In addition, the present data (see Fig. 4) show that the faster modulation of the outer peaks seen *in vitro* (14) also occurs *in vivo*. At the present timing of the PRESS sequence, the main citrate resonances have a relative maximal signal amplitude at a *TE* of approximately 130 ms, whereas the amplitudes of the outer peaks are minimal (14, 21).

Apparent Relaxation Times. In three volunteers, we were able to perform inversion-recovery experiments to get an estimate of the effective T_1 of the proton spins of some compounds. In the localization scheme *TE* was set to 135 ms. Fig. 5 shows spectra of such an experiment. Resonance integrals were determined by computer integration as described in the next section. The mean effective T_1 obtained from these experiments was 339 ± 42 ms for the main component of the citrate signal complex and 837 ± 89 and 864 ± 98 ms for the methyl protons of cholines and creatine, respectively. By the same procedure the mean effective T_1 of the water proton spins in the same volume elements of the three volunteers was 1481 ± 109 ms. For comparison the effective T_1 value of the main resonance component of citrate in the phantom was also determined at $TE = 135$ ms. This T_1 increases with temperature: e.g., at 22°C a value of 360 ± 5 ms and at 32°C a value of 534 ± 8 ms was found.

Apparent T_2 relaxation times of metabolite resonances were derived from PRESS localization experiments with four different *TE*s (from 65 to 270 ms) as shown in Fig. 4. The mean values obtained for the choline and creatine signals were 227 ± 61 ms and 209 ± 97 ms, respectively ($n = 3$). To estimate the apparent T_2 of H_2O spins five or six different *TE*s between 30 and 270 ms were used. An average apparent T_2 value of 98 ± 9 ms was found ($n = 4$). To derive a T_2-relaxation time for the citrate methylene proton spins is more difficult as its signals follow a complicated *J* modulation using a PRESS localization scheme (14,22). The treatment of this problem for

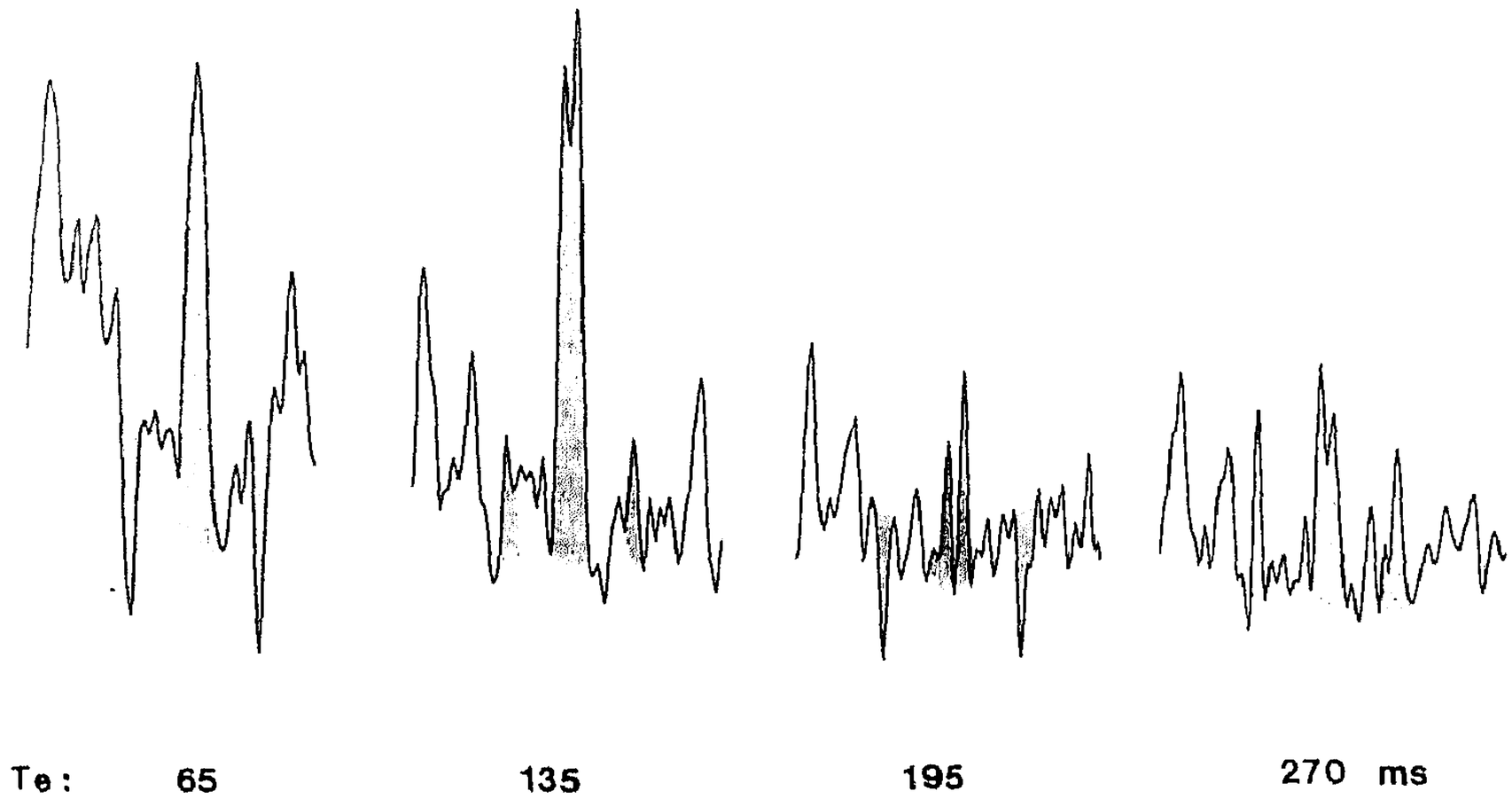

FIG. 4. MR spectra of the prostate of a volunteer obtained at different *TE*s. Nominal size of the selected volume was 5.8 cc. The *TR* was 2000 ms. To aid visualization of the modulation of citrate resonances, only the spectral part between 2.2 and 3.3 ppm is plotted. The multiplet of citrate is shaded grey. *TE*s are indicated below the spectra. The same Gaussian filter was applied to all the spectra.

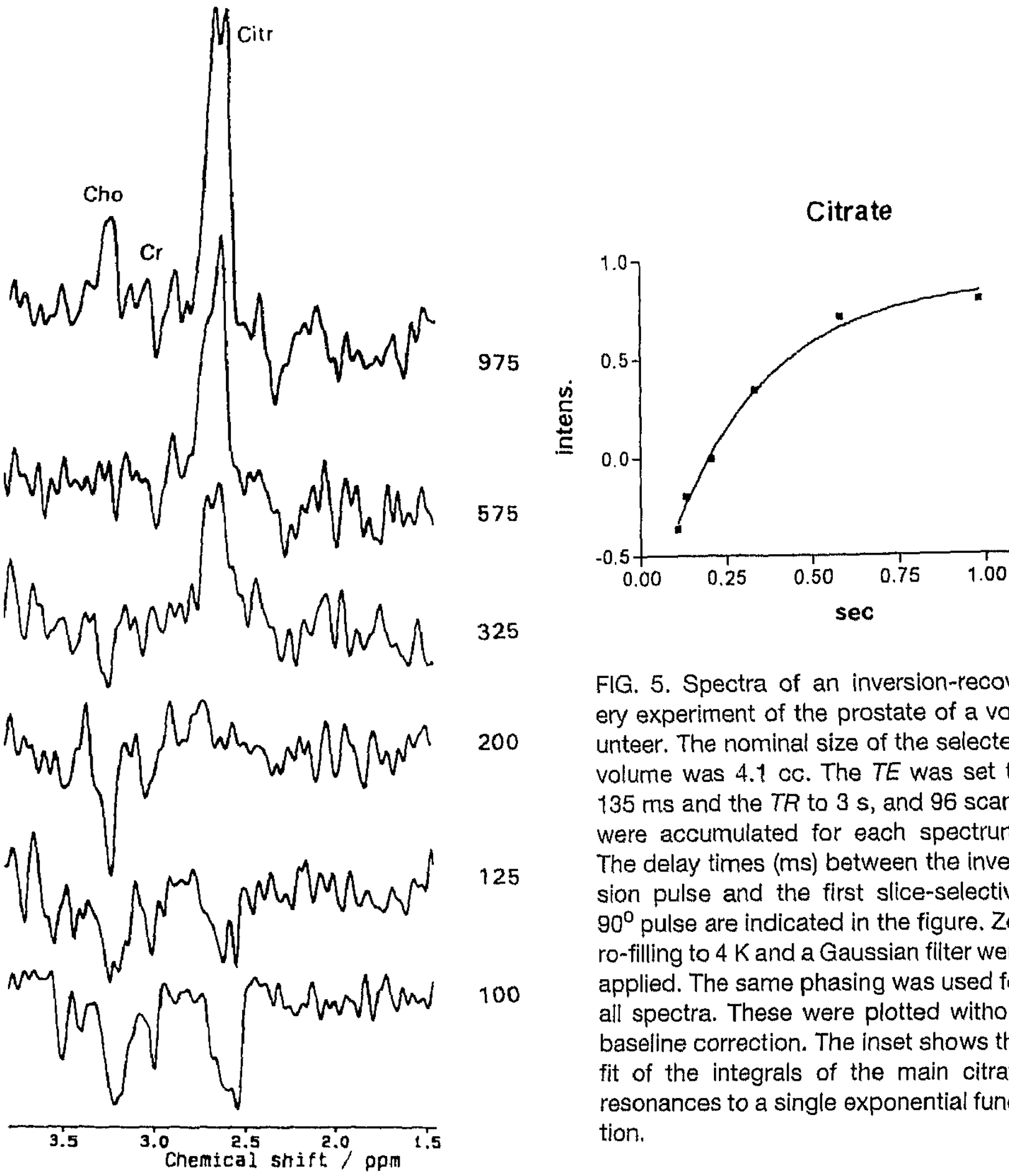

FIG. 5. Spectra of an inversion-recovery experiment of the prostate of a volunteer. The nominal size of the selected volume was 4.1 cc. The *TE* was set to 135 ms and the *TR* to 3 s, and 96 scans were accumulated for each spectrum. The delay times (ms) between the inversion pulse and the first slice-selective 90° pulse are indicated in the figure. Zero-filling to 4 K and a Gaussian filter were applied. The same phasing was used for all spectra. These were plotted without baseline correction. The inset shows the fit of the integrals of the main citrate resonances to a single exponential function.

the interpretation of *in vivo* MR results will be the subject of a separate publication.

Quantitation. The good resolution of the spectra obtained at a *TE* of 135 ms allowed evaluation of the integrals of the resonances of cholines and creatine and of the main component of the citrate multiplet.

Integration of resonances in the frequency domain was performed in two different ways after Gaussian filtering and phasing. Gaussian filtering consisted of a 2-Hz Lorentzian linewidth removal and a 4-Hz Gaussian linewidth broadening. Usually only minor baseline correction was needed. In the first approach signals were fitted to a Gaussian model function. In the second approach the signal areas were obtained by computer integration. Integration of the main resonances of citrate was performed between the spectral limits of 2.49 and 2.77 ppm, of the creatine methyl peak between 2.96 and 3.11 ppm, of the choline methyl peak between 3.12 and 3.30 ppm, and of the water resonance between 4.42 and 4.94 ppm. The data were first evaluated as signal ratios. Because *TR*s of the experiments varied between 1.6 and 4.5 s, the resonance integrals have been corrected with the effective T_1 values given above. Figure 6 displays individual values for the ratios of citrate and cholines, cholines and creatine, and citrate and the sum of cholines and creatine, as obtained by the signal-fitting procedure. Note that the highest citrate ratios are observed for the two largest volumes measured. In the measurement of the volunteer at 25 years of age, a nominal voxel size of 5.8 cc was selected, and in the second measurement of the volunteer at 32 years of age, a nominal voxel size of 4.1 cc was selected. The lowest citrate ratio was determined for the volume estimated to be the least contaminated with peripheral zone tissue, i.e., in the first measurement of the volunteer at 32 years of age.

Table 1 (Column I) gives the average values of ratios obtained from all single voxel examinations at a *TE* of 135 ms. The ratio calculations from computer integration of signals gave very similar results, i.e., citrate/choline, citrate/(choline + creatine), and choline/creatine were 2.10 ± 0.74, 1.47 ± 0.49, and 2.44 ± 0.50, respectively. Column II gives the average ratios only including spectra from nominal volumes of 3.4 cc.

Because we also have recorded the H_2O signal for all volumes of which a spectrum was obtained, it is in principle possible to estimate tissue concentrations of metabolites using water as an internal reference. For this estimation, it was assumed that the water content of prostate tissue is 83% and the tissue density 1.02 kg/liter (23).

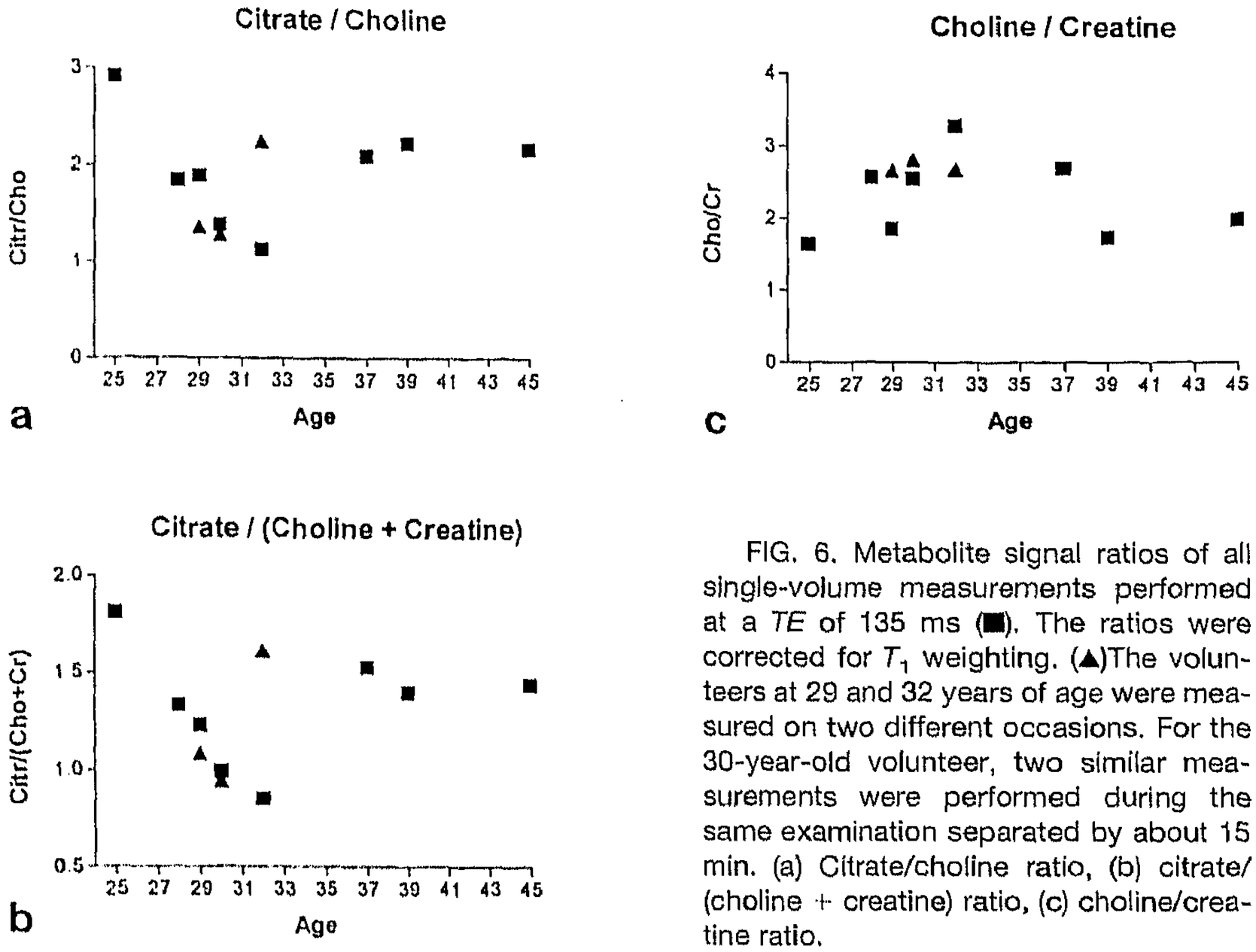

FIG. 6. Metabolite signal ratios of all single-volume measurements performed at a *TE* of 135 ms (■). The ratios were corrected for T_1 weighting. (▲)The volunteers at 29 and 32 years of age were measured on two different occasions. For the 30-year-old volunteer, two similar measurements were performed during the same examination separated by about 15 min. (a) Citrate/choline ratio, (b) citrate/(choline + creatine) ratio, (c) choline/creatine ratio.

Furthermore, it was arbitrarily assumed that 10% of tissue water is not recovered in the H_2O resonance of the MR recording at *TE* = 135 ms because of a short T_2, e.g., because of macromolecular binding and other interactions, similar to that described for brain MR studies (24). By these calculations, the average prostate tissue concentrations (per liter of tissue volume) of cholines and creatine were estimated to be 3.1 ± 0.7 and 4.4 ± 0.8 m*M*, respectively (n = 10).

SI Measurements

Phantom Study. Figure 7a shows a transversal MR image of the phantom also displaying the preselected volume and the grid with SI voxels. The MRI intensity distribution within the sphere follows the sensitivity profile of the endorectal coil. Figure 7b shows spectra obtained from the voxels within the preselected volume. The spectrum in the lower right corner only shows signal intensity arising from lipid protons of sunflower oil as expected for its location. Spectra of voxels completely located within the sphere show signals for citrate, glycine, and acetate. Signal intensity varies as a function of the sensitivity of the surface coil. Notice that the outer lines of the citrate multiplet are nearly in antiphase, which is in contrast with the single-voxel measurements where the outer lines are more in phase. This is because of the difference in time between the 90° and first 180° slice-selection pulses. The small, sometimes inverted lipid signals seen in the SI spectra are attributed to voxel bleeding. Spectra of voxels located partly in the sphere and partly outside show signal contributions of citrate, glycine, and acetate compounds and of lipids according to their partial-volume extent of sphere and container. These results illustrate the quality of localization by the present SI approach.

Volunteer Studies. For the preselected volumes chosen in this study (about 12 cc), we obtained a H_2O resonance linewidth at half maximum just below 10 Hz, which appeared to be sufficient to obtain well-resolved signals in most voxels of the spectroscopic images.

Table 1
Average Metabolite Signal Ratios of Normal Human Prostate ^{1}H MR Spectra

Ratio	I[a]	II[b]	III[c]	IV[d]
Citrate/choline	1.91 ± 0.54	1.74 ± 0.43	1.46 ± 0.23	2.89 ± 0.68
Citrate/(choline + creatine)	1.33 ± 0.30	1.22 ± 0.24	0.94 ± 0.16	1.88 ± 0.34
Choline/creatine	2.37 ± 0.54	2.43 ± 0.53	1.91 ± 0.57	1.85 ± 0.64

Average ratios of signal integrals (± SD) at *TE* = 135 ms. Corrections were made for T_1 weighting using the effective T_1 values derived from inversion-recovery experiments as described in the text.
[a] Ratios obtained from integrals of Gaussian lineshape-fitted signals as described in Materials and Methods section. A total of eight volunteers were investigated. For one volunteer, two spectra of the same volume were obtained at different moments (about 15 min apart) during the same investigation. The average of these measurements was included in the calculation as a single data point. Two other volunteers were investigated twice at different occasions. The data points obtained from both these investigations were included in the calculation. This sums up to n = 10.
[b] Same as Column I, but excluding spectra obtained from nominal volumes larger than 3.4 cc (1.5 × 1.5 × 1.5 cm). For this column, n = 8.
[c] Average ratios of signal integrals of spectra from volumes of about 1 cc located in the central/transition zone of the prostate derived from ^{1}H SI experiments (n = 4). Spectral lines were fitted to a Gaussian lineshape function.
[d] Same, but from the peripheral zone of the prostate.

the sphere and the container. (b) ^{1}H MR spectra of the voxels in the preselected volume. The orientation is the same as that for Fig. 7A. The nearly coinciding main citrate signals (Ci) and signals of acetate (Ac) and glycine (Gl) are indicated in the middle left voxel. The major lipid signals are indicated by "Lip" in the lower right voxel. Spectra are plotted from 0 to 4 ppm.

Figure 8 displays a transversal T_2-weighted image through the prostate of a 32-year-old volunteer at a level close to the veramontanum. Anatomical details such as peripheral zone, central gland, and capsule are visible. Because of the youth of the volunteer, the prostate is relatively small, and distinction between peripheral zone and central gland is less prominent than that usually seen at older age. The grid projected on the image identifies voxels from which spectra are displayed in Fig. 9. These voxels have been obtained after extrapolating spatial data from a 16×16 to a 32×32 matrix by zero-filling in two dimensions in k-space before Fourier transformation.

Figure 9 shows spectra from voxels in the black-lined block in Fig. 8. Other voxels from the preselected volume show almost only signals for periprostatic fat. Typical spectral profiles observed in the selected data set appear to be related to prominent features of the human prostate. High triglyceride signals are observed outside the prostate or at the capsule, so most of the intensity in the upper row comes from triglycerides and very little from prostate metabolites. Note the relative decrease of the triglyceride signal in the two middle spectra of this row, which coincide with the location of the anterior fibromuscular band, which has a low signal intensity on T_1- and T_2-weighted MRI (25, 26). The left column also

mined in the single-voxel measurements. The T_1-corrected values are shown in Table 1, Columns III and IV. The citrate signal ratios are significantly higher in peripheral gland compared with central gland. The values

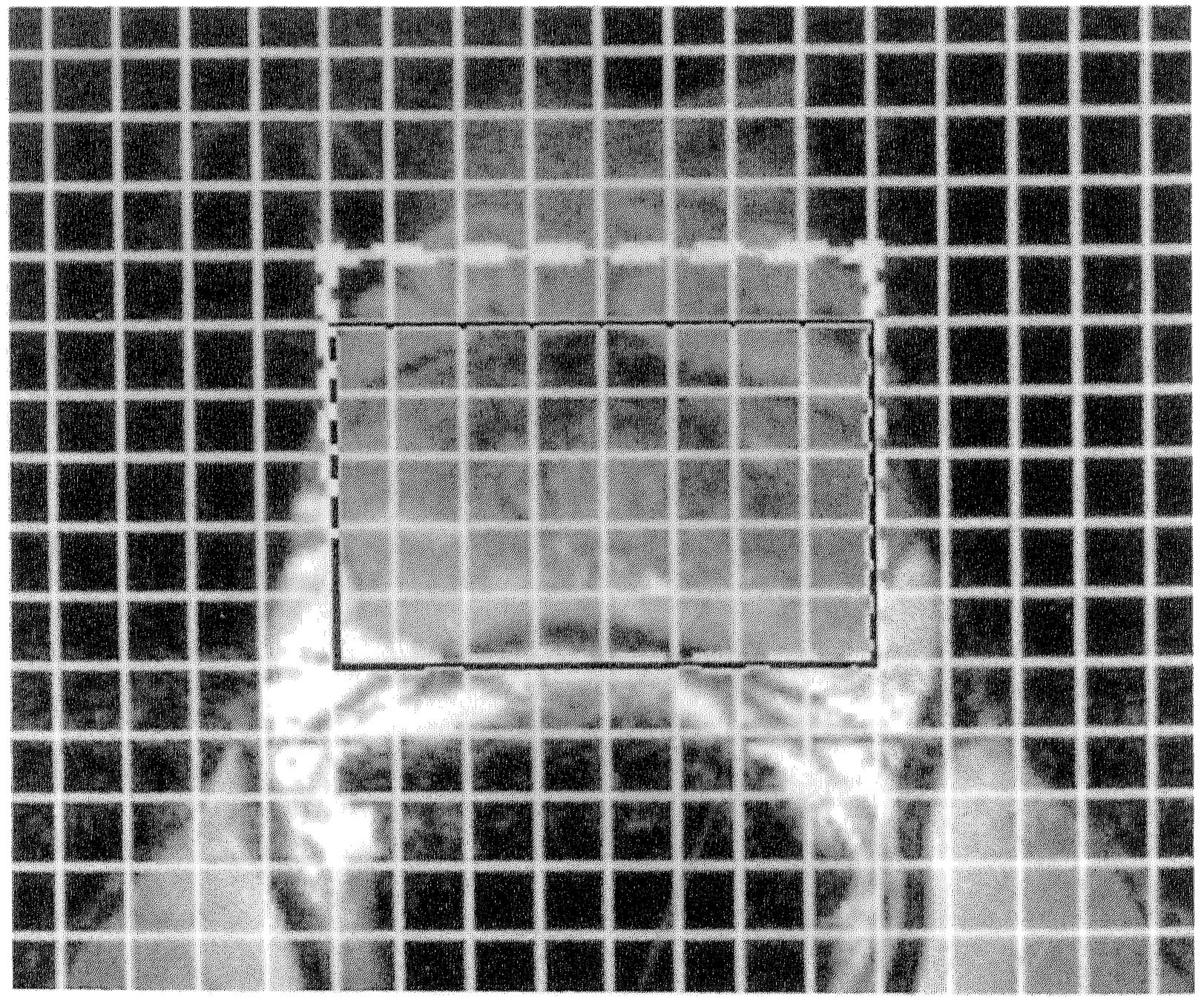

FIG. 8. Transversal MR image showing the prostate of a 32-year-old healthy volunteer. The slice thickness was 5 mm. SI was performed for an 11-mm-thick transversal plane. It was centered at the same position, but extended about 3 mm at either side beyond the MRI slice borders. The preselected PRESS volume is indicated by the white dashed box. Zero-filling in the spatial dimensions has been performed from a 16×16 to a 32×32 matrix. The volume with voxels from which spectra are displayed in Fig. 9 are indicated by a solid black box.

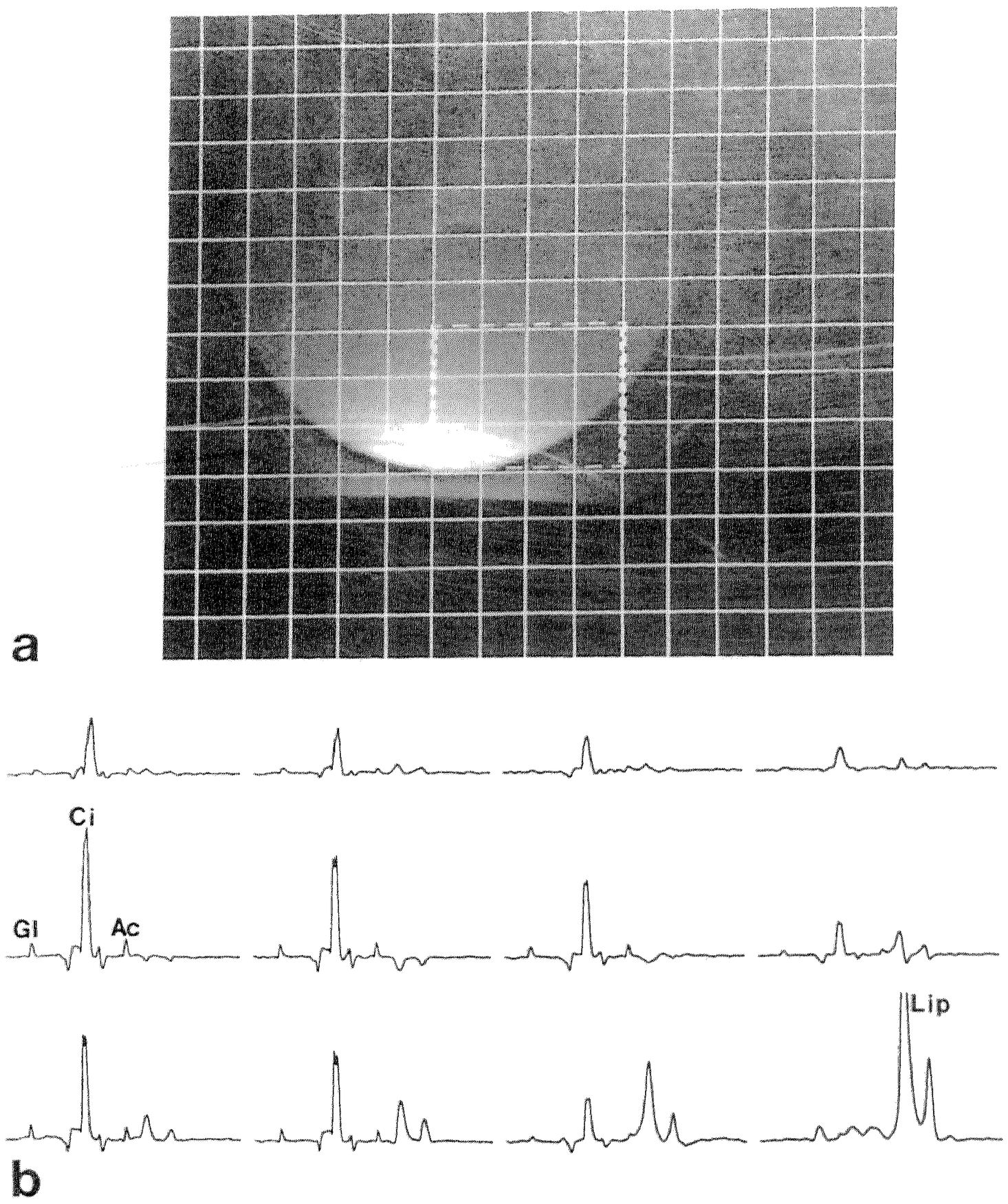

FIG. 7. (a) Transversal MR image of the test phantom. At the same position, an 11-mm–thick slice was selected for SI. The grid indicates voxels from which spectra have been acquired. The dashed line delineates the preselected volume, which is both in

shows spectra mainly with signals of methylene triglyceride protons of periprostatic fat. In the second row from above, signals of metabolites in the prostate become visible, such as those for citrate methylene protons (at 2.63 ppm) and choline and creatine methyl protons (at 3.21 and 3.03 ppm, respectively). Citrate signals are not observed outside the prostate.

Figure 10 shows enlargements of spectra from the peripheral part of the prostate (a) and from the central gland area (b). Well-resolved resonances for methylene protons of citrate and for methyl protons of creatine and (phospho)cholines can be observed. The central gland area in the selected slab predominantly is composed of the transition zone of the prostate, but it also includes a part of the central zone, urethra, periurethral tissue, and the fibromuscular band (25, 26). Notice that in both spectra the outer lines of citrate are nearly in antiphase, like those found for the citrate signal in the phantom study.

Spectroscopic images of similar quality to those illustrated above were obtained from prostate of three other volunteers (age range, 40 to 46 years). In all four volunteers, voxels of 1 cc were selected both from the peripheral zone and the central/transition zone. In the latter voxels, contamination with peripheral zone tissue was estimated to be less than 10%. The citrate/cholines, citrate/(cholines + creatine), and cholines/creatine signal integral ratios were determined by fitting of the spectral lines to Gaussian model functions. T_1 corrections were performed assuming similar apparent T_1 values for proton spins in peripheral and central gland as those deter-

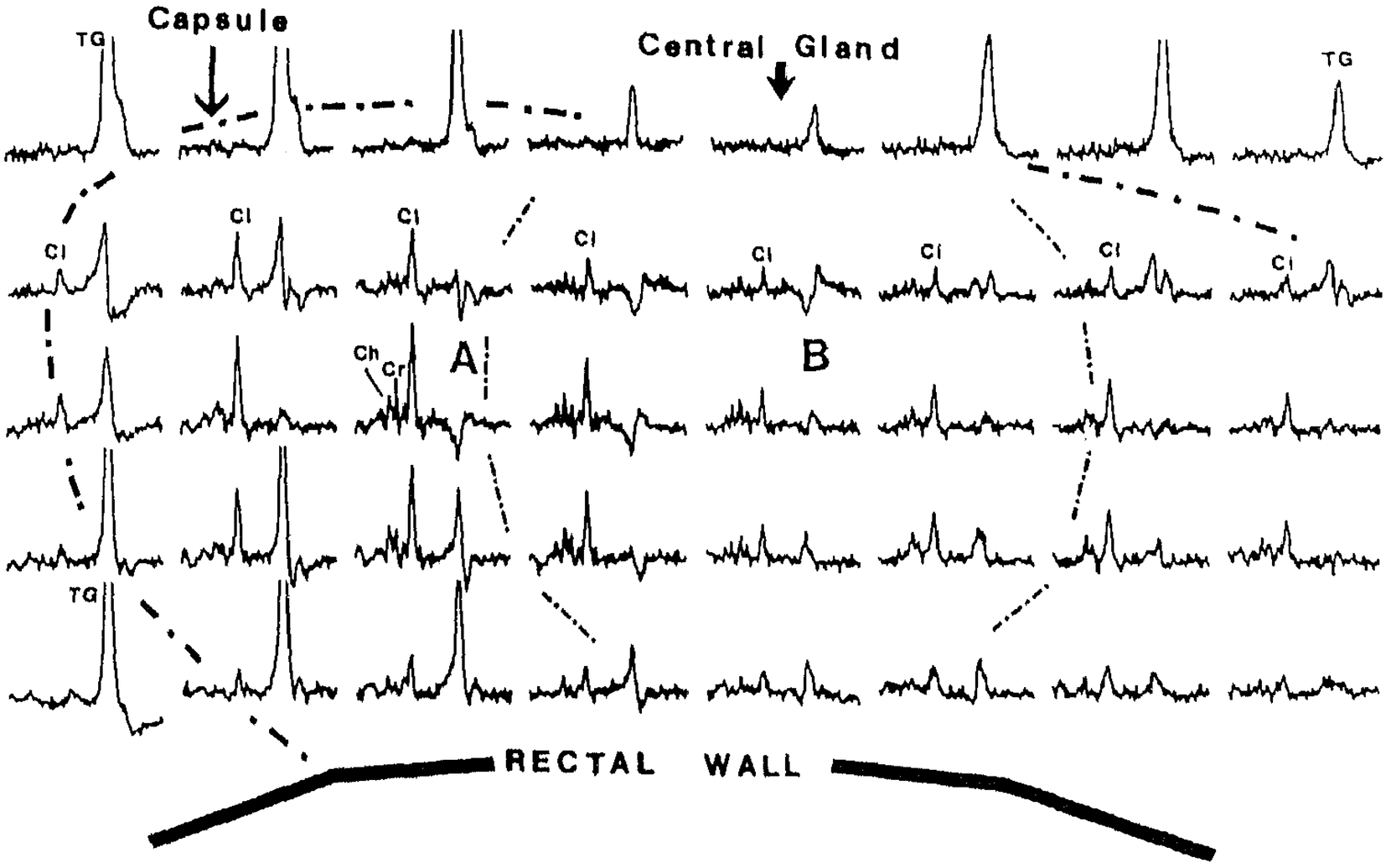

FIG. 9. Spectra of an SI data set from the voxels as shown in Fig. 8 (black box). The maximum of the Gaussian filter applied was 64 ms and the half-width 256 ms. To aid interpretation, the most prominent features of prostate anatomy are indicated schematically. Triglyceride signals are indicated by TG in the top corner spectra and in the bottom left spectrum. In the second row, the central citrate resonance in the spectra are indicated by Ci. In the spectrum labeled A, the methyl resonances for creatine (Cr) and choline (Ch) are indicated. Spectra are plotted from 0.1 to 4.1 ppm.

for average citrate ratios of the central gland (Column III) are closest to the values of citrate ratios obtained from single voxels (Column II), which were deliberately positioned in the center of the prostate.

Pulse lengths and τ value in the PRESS sequence used for single-volume acquisition are different from those used for SI experiments. Because this may affect the citrate signal, we have compared both sequences in a study of the phantom. In these experiments, the area of the main citrate signal with respect to those of the acetate and glycine resonances differed not more than 10% between both acquisition methods.

DISCUSSION

In this study, it is demonstrated that high-quality ^{1}H MR spectra can be recorded of the human prostate by the application of PRESS localization and an endorectal surface coil. Results are presented of normal prostates in volunteers at an age before BPH starts to occur.

Most experiments were performed with a timing of the PRESS sequence (i.e., TE = 135 ms), which is nearly optimal for refocusing of the main multiplet signals of citrate and which in principle enables one to identify lactate signals if present. Spectra obtained at this TE are also sufficiently depleted of broad components to enable quantitative evaluation of metabolite signals. ^{1}H MRS of volumes carefully located in the center of the prostate demonstrate that it is possible to obtain spectra with few or no signals between 0.5 and 2 ppm. High signal intensity in this chemical-shift range, often seen in ^{1}H MR spectra of the prostate *in vivo*, is likely dominated by contamination of triglyceride signals from periprostatic fat.

The spectra obtained at TE = 135 ms show almost only signal intensity for the methyl protons of cholines and creatine next to the dominating peak of citrate methylene protons. The presence of signals of these compounds could be anticipated from *in vitro* extract studies, e.g. (8, 10–12). However, these studies also revealed the presence of other compounds in prostate tissue at comparable amounts, e.g. inositol, taurine, glutamine, and glutamate

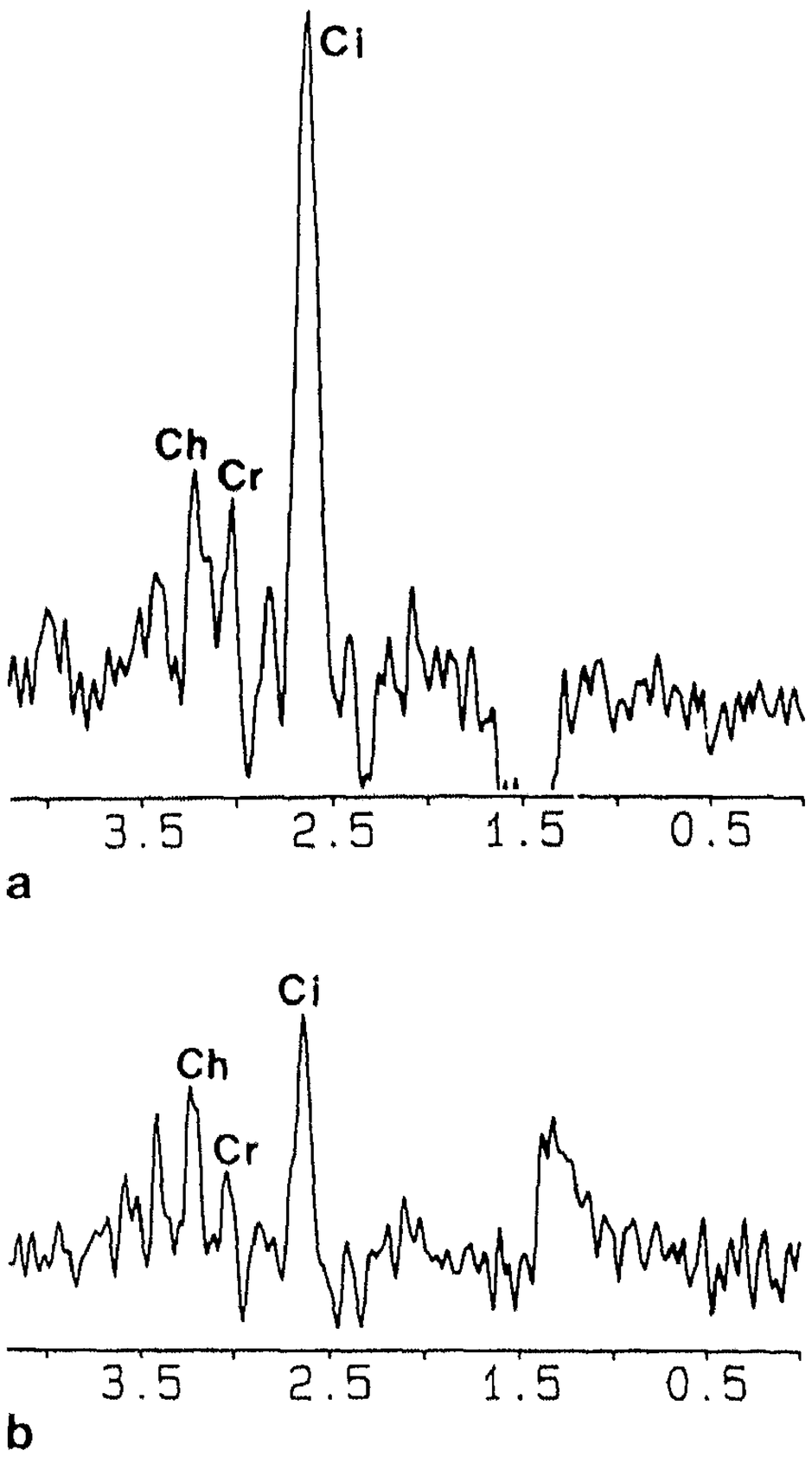

FIG. 10. (a) ^{1}H MR spectrum of the peripheral part of the prostate. It is a blowup from the spectrum labeled A in the third row of Fig. 9. (b) ^{1}H MR spectrum of the central prostate gland. This spectrum is a blowup of a spectrum from the same row labeled (b).

and possibly polyamines. Because of T_2 relaxation and/or J modulation, their signals are much attenuated in spectra obtained at TE = 135 ms. However, at shorter TEs, additional signals appear that can be assigned to some of these compounds. In this respect, the situation is much the same as for ^{1}H MR spectra of the brain obtained by the PRESS sequence. At longer TEs, signals for choline, creatine and *N*-acetylaspartate are essentially the only signals remaining in the spectra.

In ^{1}H NMR spectra of extracts of normal prostate tissue, significant signals are observed for lactate (12,13). However, the present *in vivo* results, obtained by single-voxel acquisition at TE = 135 ms, give no indication for such signals. Lactate may have become "NMR invisible" *in vivo*, for instance because of macromolecular binding, but more likely its presence in *in vitro* spectra is a consequence of the biopsy procedure.

A study concerning normal prostate has been reported in which PRESS was used for localization in conjunction with a Helmholtz coil for signal reception (14). In concurrence with our findings, no signs for the presence of a lactate signal in spectra of the prostate were observed. Furthermore, slow J modulation of the main peaks of citrate *in vivo* was demonstrated. Because of improved resolution, both this slow modulation as well as the faster modulation of the outer peaks of citrate could be monitored in the present study.

It is known that substantial amounts of divalent cations such as Mg^{2+}, Ca^{2+}, and Zn^{2+} are present in prostatic fluid (18). As observed in ^{1}H NMR spectra of citrate solutions, both the spin-spin coupling constant and the chemical-shift positions of citrate signals are sensitive to pH, but much more to complexation of citrate with these cations (27). The chemical-shift positions of citrate signals measured *in vivo* are similar to those measured *in vitro* in the presence of divalent cations, which indicates that, in the prostate as well, citrate is complexed to these ions.

In a few volunteers, apparent relaxation times for water and metabolite proton spins in the prostate have been estimated. T_1 and T_2 relaxation times for water proton spins are close to values published previously by Kjaer *et al.* (28). Recently, spatially more precise T_2 measurements have been made showing a longer T_2 relaxation time for the peripheral zone compared with that of the central zone (29). Our T_2 value is closest to that reported for the central zone, which is in agreement with the location of the volumes from which the measurements have been made. The apparent T_1 and T_2 relaxation times estimated for choline and creatine methyl proton spins are equal or somewhat shorter than T_1 and T_2 relaxation times of the corresponding proton spins in ^{1}H spectra of the adult human brain (30). For citrate methylene proton spins, a relatively short effective T_1 value is found. As citrate efficiently binds divalent cations (27), this may be caused by trace amounts of paramagnetic ions. The estimation of these relaxation times provides starting values to set sequence timing in ^{1}H MRS studies of the prostate and to enable quantification of compound levels.

Presently, few quantitative data of localized ^{1}H MRS of the healthy human prostate *in situ* are available. Most studies have been performed using the STEAM localization sequence (4, 9, 13, 29, 31). In a recent study by Kurhanewicz *et al.* (32), quantitative data on the ratio of the citrate signal with respect to signal intensity at the choline and creatine position in spectra of zonal regions of healthy volunteers are presented using both STEAM and PRESS. Although experimental and processing conditions are somewhat different from ours, the mean ratios in both studies are fairly similar. Some estimates of the tissue content of citrate in the prostate have been made by localized ^{1}H MRS (5, 29), but adequate evaluation of the complex citrate signal and correction for J modulation and T_2 relaxation for this purpose have not been fully realized yet.

Levels for choline and creatine compounds in the prostate have not been reported until now. The concentrations for cholines and creatine in the prostate estimated by MRS in the present study are different from those determined for brain tissue by the same method. The estimated choline concentration is higher and the creatine concentration lower than that found in brain (30). A substantial part of creatine in the prostate is phosphorylated (12, 33, 34). The most likely locations for creatine are the various smooth-muscle components in the prostate, i.e., stromal and capsular muscle cells and myoepithelial cells surrounding prostatic acini.

Previously, we performed ^{1}H NMR of an extract of a normal prostate tissue specimen (12). We reanalyzed data of this sample to enable comparison with the present *in vivo* results. From a fully relaxed ^{1}H NMR spectrum obtained from the sample at pH 7, the total creatine signal intensity (Cr) was determined. Furthermore the signal intensity between 3.15 and 3.28 ppm was determined, including contributions of all methyl protons of various choline compounds (Cho) but excluding contributions of taurine, inositol, and phosphoethanolamine protons. A Cho/Cr ratio of 1.81 was found that is only slightly lower than the Cho/Cr ratio obtained by *in vivo* MRS measurements at TE = 135 ms. Because Cho and Cr methyl proton spins have similar T_2 values, this indicates that the majority of signal intensity at about 3.2 ppm seen in spectra obtained *in vivo* at TE = 135 ms originates from choline compounds.

The results of the SI experiments show that high-quality spectra can be obtained simultaneously from multiple locations in the prostate. The present acquisition time to record a SI data set with good signal-to-noise ratio at a nominal resolution of 1 cc was 13.6 min at a TR of 1600 ms. Obviously, based on the estimations of the effective T_1 relaxation times of the main resonances, a better signal-to-noise ratio per unit time can be achieved and thus spatial resolution may be enhanced. The acquisition of ^{1}H MR spectra of the human prostate at a spatial resolution below 1 cc has been demonstrated to be possible (32,35). Such resolution may be needed to match with the complex anatomy of the human prostate and with the heterogeneity of prostate pathology.

Variations in resonance intensity for distinct morphological locations in the prostate become visible at a spatial resolution of about 1 cc. Most striking is the lower relative level of the citrate signal in spectra from the central/transition zone as compared to the peripheral zone. Recently, a similar difference in citrate signal levels between peripheral zone and central/transition zone

has been observed in other MRS studies (29, 32). The average citrate content in the peripheral part of the prostate appears to be twice of the amount in the central part (29). The same increase is found for the relative citrate signal in the present study. A higher citrate level in the peripheral zone presumably is related to the presence of more glandular elements in this area (25). This also explains why in the single-volume measurements the citrate ratios are the highest in cases with most contributions of peripheral zone tissue.

In conclusion, this study on healthy individuals shows that, with PRESS localization and an endorectal coil, it is possible to perform detailed MR spectroscopic investigations of a number of metabolites in relevant parts of the human prostate. Data obtained in this way may serve as a reference for clinical applications of ^{1}H MRS to BPH and prostate cancer (32, 35).

ACKNOWLEDGMENTS

We thank Dr. Sauter and co-workers at Siemens Erlangen, Germany, for providing us with an elementary proton SI pulse sequence and postprocessing software. Furthermore, we thank Ing. H. J. van den Boogert for technical assistance and Dr. W. M. M. J. Bovée (Technical University of Delft) for useful discussions.

REFERENCES

1. M. D. Schnall, R. L. Lenkinski, H. M. Pollack, Y. Imai, H. Y. Kressel, Prostate: MR imaging with an endorectal surface coil. *Radiology* **172**, 570–574 (1989).
2. P. Narayan, D. B. Vigneron, P. M. Jajodia, C. M. Anderson, M. W. Hodgcock, E. A. Tanagho, T. L. James, Transrectal probe for ^{1}H MRI and ^{31}P MR spectroscopy of the prostate gland. *Magn. Reson. Med.* **11**, 209–220 (1989).
3. M. A. Thomas, P. Narayan, J. Kurhanowicz, P. Jojadia, M. W. Weiner, ^{1}H MR Spectroscopy of normal and malignant human prostates *in vivo*. *J. Magn. Reson.* **871**, 610–619 (1990).
4. M. Schnall, R. Lenkinski, B. Milestone, H. Kressel, Localized ^{1}H spectroscopy of the human prostate *in vivo*, *in* "Proc., SMRM, 9th Annual Meeting, New York, 1990," p. 288.
5. A. Heerschap, G. Jager, A. de Koster, J. Barentsz, J. de la Rosette, F. Debruyne, J. Ruijs, ^{1}H MRS of prostate pathology, *in* "Proc., SMRM, 12th Annual Meeting, New York, 1993," p. 213.
6. L. C. Costello, R. B. Franklin, Concepts of citrate production and secretion by prostate: 1. Metabolic relationships. *Prostate* **18**, 25–46 (1991).
7. K. R. Halliday, C. Fenoglio-Preiser, L. O. Sillerud, Differentiation of human tumors from nonmalignant tissue by natural-abundance ^{13}C NMR spectroscopy. *Magn. Reson. Med.* **7**, 384–411 (1988).
8. A. H. Fowler, A. A. Pappas, J. C. Holder, A. E. Finkbeiner, G. V. Dalrymple, M. S. Mullins, J. R. Sprigg, R. A. Komoroski, Differentiation of human prostate cancer from benign hypertrophy by *in vitro* ^{1}H NMR. *Magn. Reson. Med.* **25**, 140–147 (1992).
9. P. Narayan, J. Kurhanowicz, Magnetic resonance spectroscopy in prostate disease: diagnostic possibilities and future developments. *Prostate*. Supplement **4**, 43–50 (1992).
10. J. Kurhanowicz, R. Dahiya, J. M. McDonald, L. H. Chang, T. L. James, P. Narayan, Citrate alterations in primary and metastatic human prostatic adenocarcinomas: ^{1}H magnetic resonance spectroscopy and biochemical study. *Magn. Reson. Med.* **29**, 149–157 (1993).
11. M. L. Schiebler, K. K. Miyamoto, M. White, S. J. Maygarden, J. L. Mohler, *In vitro* high resolution ^{1}H spectroscopy of the human prostate: benign prostatic hyperplasia, normal peripheral zone, and adenocarcinoma. *Magn. Reson. Med.* **29**, 285–291 (1993).
12. E. B. Cornel, G. A. H. J. Smits, G. O. N. Oosterhof, H. F. M. Karthaus, F. M. J. Debruyne, J. A. Schalken, A. Heerschap, Characterization of human prostate cancer, benign prostate hyperplasia, and normal prostate by *in vitro* ^{1}H and ^{31}P magnetic resonance spectroscopy. *J. Urol.* **150**, 2019–2024 (1993).
13. J. Kurhanowicz, D. B. Vigneron, S. J. Nelson, H. J. Hricak, J. M. McDonald, B. Konety, P. Narayan, Citrate as an *in vivo* marker to discriminate prostate cancer from benign hyperplasia and normal prostate peripheral zone: detection via localized proton spectroscopy. *Urology* **45**, 459–466 (1995).
14. F. Schick, H. Bongers, S. Kurz, W.-I. Jung, M. Pfeffer, O. Lutz, Localized proton MR spectroscopy of citrate *in vitro* and of the human prostate *in vivo* at 1.5 T. *Magn. Reson. Med.* **29**, 38–43 (1993).
15. R. J. Ordidge, M. R. Bendall, R. E. Gordon, A. Connelly, Volume selection for *in vivo* biological spectroscopy, *in* "Magnetic Resonance in Biology and Medicine" (G. Govil, C. L. Khetrapal, A. Saran, Eds.), pp. 386–397, Tata McGraw-Hill, New Delhi, 1985.
16. P. A. Bottomley, Spatial localization in NMR spectroscopy *in vivo*. *Ann. N.Y. Acad. Sci.* **508**, 333–348 (1987).
17. A. Haase, J. Frahm, W. Hänicke, D. Matthaei, ^{1}H NMR chemical shift selective (CHESS) imaging. *Phys. Med. Biol.* **30**, 341–344 (1985).
18. J. P. Kavanagh, Sodium, potassium, calcium, magnesium, zinc, citrate and chloride content of human prostatic and seminal fluid. *J. Reprod. Fertil.* **75**, 35–41 (1985).
19. U. Klose, *In vivo* proton spectroscopy in presence of eddy currents. *Magn. Reson. Med.* **14**, 26–30 (1990).
20. J. E. McNeal, Normal histology of the prostate. *Am J. Surg. Pathol.* **12**, 619–633 (1988).
21. K. Straubinger, F. Schick, O. Lutz, Computer-algebra calculations and measurements on AB spin systems for double-spin-echo sequences. *MAGMA* **3**, 109–118 (1995).
22. R. V. Mulkern, J. L. Bowers, Calculating spectral modulations of AB systems during PRESS acquisition. *Magn. Reson. Med.* **30**, 518–519 (1993).
23. Report of the Task Group on the Reference Man, International Commission on Radiological Protection, no 23. Pergamon Press, New York (1981).
24. T. Ernst, R. Kreis, B. D. Ross, Absolute quantitation of water and metabolites in the human brain: I. Compartments and water. *J. Magn. Reson. B* **102**, 1–8 (1993).
25. H. Hricak, G. C. Dooms, J. E. McNeal, A. S. Mark, M. Marotti, A. Avallone, M. Pelzer, E. C. Proctor, E. A. Tanagho, MR imaging of the prostate gland: normal anatomy. *Am. J. Roentgenol.* **148**, 51–58 (1987).
26. M. D. Schnall, M. Bezzi, H. M. Pollack, H. Y. Kressel, Magnetic resonance imaging of the prostate. *Magn. Reson. Q.* **6**, 1–16 (1990).
27. M. Van der Graaf, A. Heerschap, Effect of cation binding on the proton chemical shifts and the spin-spin coupling constant of citrate. *J. Magn. Reson.* **B112**, 58–62, (1996).
28. L. Kjaer, C. Thomsen, P. Iversen, O. Henriksen, *In vivo* estimation of relaxation processes in benign hyperplasia and carcinoma of the prostate gland by magnetic resonance imaging. *Magn. Reson. Imaging* **5**, 23–30 (1987).
29. M. Lowry, D. J. Manton, L. W. Turnbull, S. J. Blackband, A. Horsman, Quantitative proton MRS assessment of citrate heterogeneity in normal prostate. *MAGMA* **2**, 483–485 (1994).
30. R. Kreis, T. Ernst, B. D. Ross, Development of the human brain: *in vivo* quantification of metabolite and water content with proton magnetic resonance spectroscopy. *Magn. Reson. Med.* **30**, 424–437 (1993).
31. M. L.Schiebler, M. D. Schnall, H. M. Pollack, R. E. Lenkinski, J. E. Tomaszewski, A. J. Wein, R. Whittington, W. Rauschning, H. Y. Kressel, Current role of MR imaging in the staging of adenocarcinoma of the prostate. *Radiology* **189**, 339–352 (1993).
32. J. Kurhanowicz, D. B. Vigneron, H. Hricak, P. Narayan, P. Carrol, S. J. Nelson, Three-dimensional H-1 SI of the *in situ* human prostate with high (0.24–0.7 cm^3) spatial resolution. *Radiology* **198**, 795–805 (1996).
33. P. Narayan, P. Jajodía, J. Kurhanowicz, A. Thomas, J. MacDonald, B. Hubosch, M. Hodgcock, C. Anderson, T. L. James, E. A. Tanagho, M. Weiner, Characterization of prostate cancer, benign prostatic hyperplasia and normal prostate using transrectal ^{31}P phosphorus magnetic resonance spectroscopy: a preliminary report. *J. Urol.* **146**, 66–74 (1991).
34. J. Kurhanowicz, A. Thomas, P. Jajodia, M. Weiner, T. L. James, D. Vigneron, P. Narayan, ^{31}P spectroscopy of the human prostate gland *in vivo* using a transrectal probe. *Magn. Reson. Med.* **22**, 404–413 (1991).
35. A. Heerschap, G. J. Jager, M. Van der Graaf, J. O. Barentsz, J. J. M. C. H. de la Rosette, G. O. N. Oosterhof, S. J. Ruijs, *In vivo* proton MR spectroscopy reveals altered metabolite content in malignant prostate tissue. *Anticancer Res.*, in press (1996).